International Journal of Automotive Technology, Vol. 7, No. 1, pp. 101–107 (2006)

1229–9138/2006/025–13

FINITE ELEMENT ANALYSIS OF A STEADY-STATE ROLLING TIRE TAKING THE EFFECT OF TREAD PATTERN INTO ACCOUNT

K. W. KIM[1),2)*]

[1)]R&D Center, Kumho Tire Co., Inc., 555 Sochon-dong, Gwangsan-gu, Gwangju 506-711, Korea
[2)]Department of Mechanical Engineering, Chonnam National University, Gwangju 500-757, Korea

(Received 18 February 2005; Revised 21 November 2005)

ABSTRACT–The force and moment simulation of a steady-state rolling tire taking the effect of tread pattern into account is described using a steady-state transport method with ABAQUS. Tread meshes can not fully consider a tread pattern because detailed tread meshes are not allowed in the steady-state transport method. Therefore, the tread elements are modeled to have orthotropic property instead of isotropic property. The force and moment simulation has been carried out for the cases of both isotropic and orthotropic properties of tread elements. Both cases of simulation results are then compared with the experimental results. It is verified that the orthotropic case is in a better agreement with the experimental result than the isotropic case. Angle effects of tread pattern have been studied by changing the orientation angle of orthotropic property of tread. It is shown that the groove angle in the tread shoulder region has a more effect on force and moment of a tire than that in the tread center region.

KEY WORDS : Force and moment, Steady-state rolling, Orthotropic modulus, Tread pattern, Tire, Finite element analysis

1. INTRODUCTION

A tire is composed of several rubber components and cord-rubber composite layers (Clark, 1982). There exists a tread pattern outside the tire which is consisted of blocks and grooves, as shown in Figure 1. Tire modeling by finite elements is very complicated due to many non-linear factors that do not occur together in other structures. Some of these factors are geometric nonlinearity, which is due to large deformation and rotation, material nonlinearity, which includes incompressible rubber materials and cord-rubber composites, and boundary nonlinearity, which is due to contact and friction between a tire and a road surface and between a tire and a rim of a wheel. Complete simulations of tire performances are still different tasks and it requires huge computation time, owing to such complex nonlinear features. Therefore, the most finite element analysis of a tire has been limited to static analysis, which includes only inflation pressure and footprint load except rolling velocity (Danielson *et al.*, 1996). In recent years, a transient finite element analysis of a tire has been studied using an explicit finite element code for including a rolling velocity with the advances of computer technology (Kim *et al.*, 2003; Chang *et al.*, 2005). However, a steady-state rolling contact analysis of a tire, which uses an implicit time integration method, has been widely used due to its effectiveness and efficiency, compared to an explicit time integration code (Kaliske *et al.*, 2002). The steady-state rolling method not only provides an efficient function for describing a rolling tire but also reduces dramatically the computation time for solving it (Faria *et al.*, 1992). A steady-state transport formulation for the tire rolling contact was implemented into ABAQUS/Standard software. But, detailed meshes for tread blocks are not allowed due to the axisymmetry assumption in the steady-state transport method. The tread elements can be modeled to have orthotropic property in order to take the effect of a tread pattern into

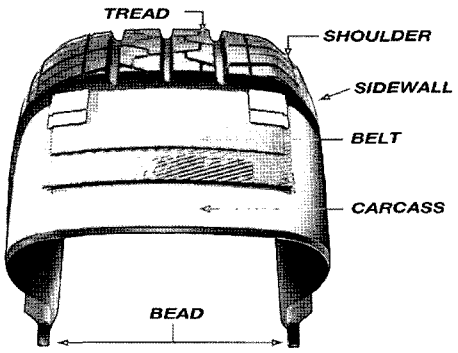

Figure 1. Tire construction and tread pattern.

*Corresponding author. e-mail: kwkim@tire.kumho.co.kr

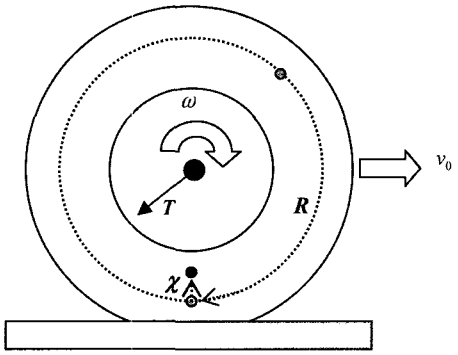

Figure 2. The configuration of steady-state rolling contact.

account. Finite element analysis of a steady-state rolling tire taking the effect of tread pattern into account is proposed in this paper.

2. STEADY-STATE ROLLING CONTACT

The rolling deformation of a tire can be divided into two consecutive motions, a rigid rotation using a Eulerian manner and then a translation using a Lagrangian manner as shown in Figure 2.

The rotation of a tire is described by a rotation matrix $\boldsymbol{R}$ in an initial configuration $\boldsymbol{X}$ and a reference configuration $\boldsymbol{Y}$. The deformation of a tire at any time t can be expressed by a map χ comparing a reference configuration and a deformed configuration. It follows that each material particle that passes position $\boldsymbol{Y}$ will experience the same displacement to $\boldsymbol{y}$ for steady-state motion.

$$\begin{aligned} \boldsymbol{Y} &= \boldsymbol{R}\cdot\boldsymbol{X} \text{ for rigid rotation} \\ \boldsymbol{y} &= \chi(\boldsymbol{Y}, t) \text{ for translation} \end{aligned} \tag{1}$$

In a reference frame attached to the axis of the wheel, the velocity $\boldsymbol{v}$ of a particle is given through the derivative of the motion and the acceleration $\boldsymbol{a}$ is obtained through the derivative of the velocity. It is known that the terms related to time derivative are removed for steady-state rolling. The remaining equations for a finite element approximation can be written without any terms related to time derivatives (ABAQUS, 2003).

$$\begin{aligned} \boldsymbol{v}(\boldsymbol{Y}, t) &= \dot{\boldsymbol{y}} = \frac{\partial \chi}{\partial \boldsymbol{Y}} \cdot \frac{\partial \boldsymbol{Y}}{\partial t} + \frac{\partial \chi}{\partial t} \\ \frac{\partial \boldsymbol{Y}}{\partial t} &= (\omega \times \boldsymbol{R}) \cdot \boldsymbol{X} = \omega(\boldsymbol{T} \times \boldsymbol{Y}) = \omega R \boldsymbol{S} \\ \boldsymbol{v}(\boldsymbol{Y}, t) &= \dot{\boldsymbol{y}} = \omega R \frac{\partial \chi}{\partial \boldsymbol{Y}} \cdot \boldsymbol{S} + \frac{\partial \chi}{\partial t} \\ \therefore \boldsymbol{v} &= \boldsymbol{v}_0 + \omega R \frac{\partial \chi}{\partial S} \\ \therefore \boldsymbol{a} &= \omega^2 R^2 \frac{\partial^2 \chi}{\partial S^2} \end{aligned} \tag{2}$$

Table 1. Comparison of explicit rolling and steady-state rolling analyses.

	Transient rolling	Steady-state rolling
Formulation	Lagrangian only	Lagrangian & Eulerian
Reference frame	Rotates with the body	Not rotate with the body
Phenomenon	Material rotates with mesh	Material only rotates
Mesh requirement	Fine meshes along the entire surface	Local fine meshes near the contact zone
Computation cost	Very expensive	Less expensive
Solving method	Explicit integration	Implicit integration
Examples	Cleat impact simulation	Force & moment simulation

where ω is angular velocity vector defined as $\omega=\omega\boldsymbol{T}$ and $\boldsymbol{S}$ is circumferential direction vector defined as $\boldsymbol{S}=(\boldsymbol{T}\times\boldsymbol{Y})/R$.

The differences between transient rolling and steady-state rolling analyses are summarized in Table 1. The steady-state rolling contact analysis permits a local fine mesh near the contact zone while the transient rolling contact analysis requires a fine mesh along the entire tire surface. It leads to large reduction of computation time in the steady-state rolling analysis. However, this analysis has a disadvantage that it can not model tread local detail meshes because the meshes in cut-section must have the same trajectories along the circum-ferential direction. Therefore, a special treatment is required to take the effect of tread pattern shapes into account.

3. TREAD ORTHOTROPIC MODULUS

As a tread pattern consists of blocks and grooves which are oriented by some angles about the axial direction of tire, tread meshes can be considered to have orthotropic property instead of isotropic property. The method to calculate the orthotropic property of tread pattern is here described. Two dimensional shape of tread pattern is displayed in Figure 3. Three dimensional tread pattern is modeled using I-DEAS software, dividing into the center and the shoulder regions. Each region consists of three pitches of the tread pattern with zero lateral groove angles and is modeled on a flat surface without considering any tread curvatures as shown in Figure 4. Then, linear finite element analyses are performed in order to calculate

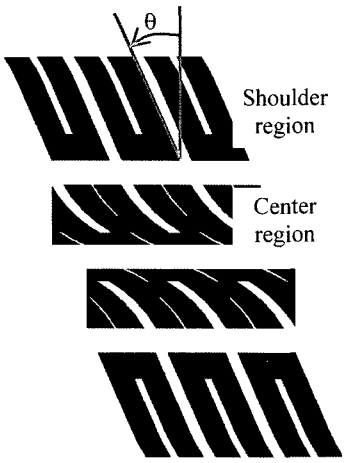

Figure 3. Two dimensional shape of tread pattern.

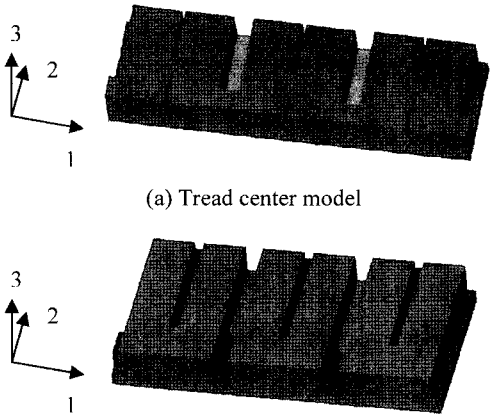

(a) Tread center model

(b) Tread shoulder model

Figure 4. Three dimensional models of tread pattern for modulus calculation.

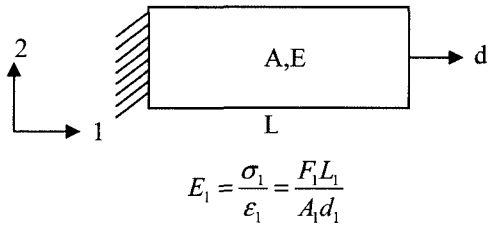

$$E_1 = \frac{\sigma_1}{\varepsilon_1} = \frac{F_1 L_1}{A_1 d_1}$$

(a) Tensile modulus calculation.

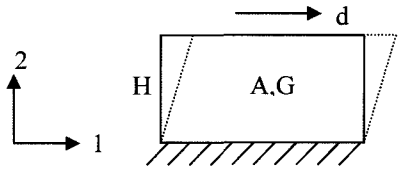

$$G_{12} = \frac{\tau_{12}}{\gamma_{12}} = \frac{F_1 H_1}{A_1 d_1}$$

(b) Shear modulus calculation.

Figure 5. Tensile and shear moduli calculation methods.

Table 2. Calculated orthotropic moduli of tread models.

unit : psi

Modulus	Isotropic	Orthotropic	
	Tread	Center	Shoulder
E_1	850	524	450
E_2	850	762	794
E_3	850	756	777
G_{12}	285	239	219
G_{23}	285	251	262
G_{13}	285	254	264

orthotropic tread moduli by applying isotropic moduli to each tread region. Tensile and shear moduli (E_i, G_{ij}) of tread regions are easily calculated from linear constitutive equations as shown in Figure 5. The calculated orthotropic moduli of each tread region are summarized in Table 2. It is found that material property of tread is not isotropic but orthotropic due to effects of tread pattern, as well as orthotropic moduli are 7~47% less than isotropic moduli.

4. TIRE FINITE ELEMENT MODEL

A passenger car's radial tire of 185/70R14 is used for simulating force and moment, and frictional energy. The finite element model of tire consists of 10,500 nodes and 9,300 elements with local fine meshes near the contact zone, as shown in Figure 6.

Rubber components except tread are modeled by solid elements with hyperelastic material of Mooney-Rivlin form as follows;

$$U = C_{10}(\bar{I}_1 - 3) + C_{01}(\bar{I}_2 - 3) + \frac{1}{D}(J-1)^2 \qquad (3)$$

where C_{ij} are the material constants related to deviatoric deformation, D is the material constant related to volumetric deformation, $\bar{I}_i$ are the stress invariants of deviatoric deformation, and J is the elastic volume expansion ratio. Tread is modeled as elastic material with linear orthotropic moduli which have been calculated already in the previous section.

Fiber reinforcement is modeled by the REBAR (ABAQUS, 2003), which is embedded in solid elements, with bi-linear modulus.

$$U = \frac{1}{2} A K \varepsilon^2$$

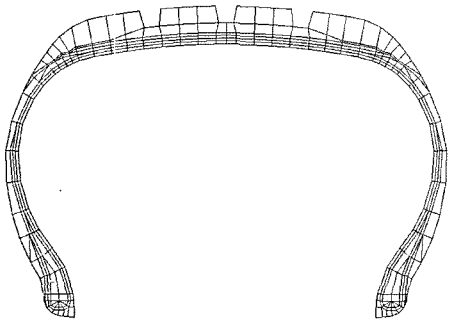

(a) Cut-section view of tire model

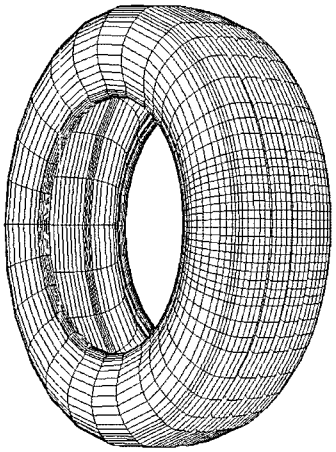

(b) Isoparametric view of tire model

Figure 6. Finite element model of tire.

Table 3. Rubber material properties.

	E (psi)	C10	C01
Tread	850	113.3	28.3
Side	570	76.0	19.0
Apex	1,950	260.0	65.0
Flange	1,210	161.3	40.3
Bead	12,484,000	–	–

$$\varepsilon = \frac{1}{2}\frac{(d\boldsymbol{s}\cdot d\boldsymbol{s} - d\boldsymbol{S}\cdot d\boldsymbol{S})}{d\boldsymbol{S}\cdot d\boldsymbol{S}} \tag{4}$$

where A is the area, K is the elastic modulus, ε is the strain, $d\boldsymbol{s}$ and $d\boldsymbol{S}$ are the original and deformed configurations of the cord elements respectively.

The Inflation pressure of 193.05 kPa (28 psi) is applied inside the tire and the vertical footprint load of 410 kgf (903.88 lbf) is applied to the road surface. The coefficient of friction is applied as 1.0 between the tire and the road surfaces. The travel velocity of the tire is 3.2 km/h for the force and moment simulation, and the frictional energy simulation, which is the same velocity as that of each test machine. The slip angle is changed from −6 to +6 degrees, which is the same slip angle as that of test machine, to calculate force and moment characteristics.

Table 4. Cord material properties.

	E (psi)	Angle (°)	EPI
Belt	1.603E7	+21/−21	18.0
Carcass	3.937E5	90	28.0
Cap ply	2.300E5	0	22.0

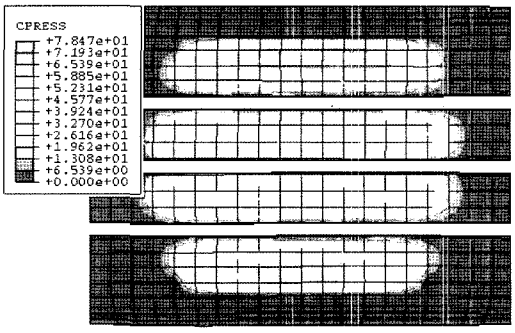

(a) Footprint pressure of the isotropic tread model

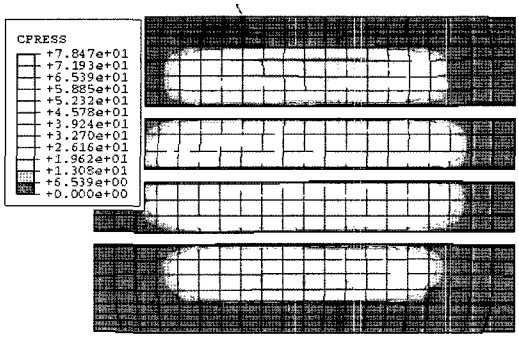

(b) Footprint pressure of the orthotropic tread model

Figure 7. Footprint pressure distributions in the straight rolling analyses.

5. FOOTPRINT PRESSURE SIMULATION

Footprint pressure simulations are conducted for investigating an effect of orthotropic property of tread. Footprint pressure distributions on straight rolling and cornering conditions are shown in Figure 7 and Figure 8 respectively. Footprint pressure distributions of orthotropic tread model are almost same as those of the isotropic one. It is found that the loss of contact patch does not happen in the straight rolling status but it occurs at the outside shoulder region in the cornering status.

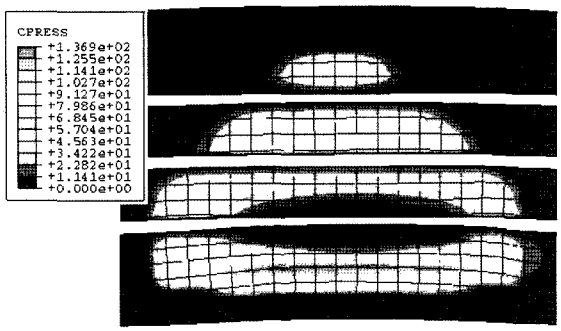

(a) Footprint pressure of the isotropic tread model

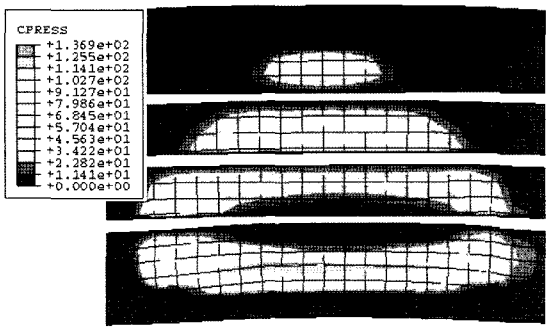

(b) Footprint pressure of the orthotropic tread model

Figure 8. Footprint pressure distributions in the cornering analyses (slip angle 6×).

6. FORCE AND MOMENT SIMULATION

When tire is rolling on road with slip angle, lateral force and aligning moment are occurred by interaction between tire and road as shown in Figure 9. The aligning moment is calculated by multiplying the lateral force by the pneumatic trail as follows;

$$M_z = t_p \times F_y \tag{5}$$

where M_z is aligning moment, t_p is pneumatic trail, and F_z is lateral force.

The calculated results on force and moment characteristics are summarized in Table 3 and the graphs on lateral forces and aligning torques are displayed in Figure 10. The cornering coefficient (CC) is calculated by dividing lateral force by vertical load and the aligning torque coefficient (ATC) is calculated by dividing aligning torque by vertical load. The plysteer residual aligning torque (PRAT) equals to aligning torque at a slip angle where lateral force is zero.

The cornering coefficients are little influenced by tread material model, while the aligning torque and the plysteer residual aligning torque by the orthotropic tread model are in better agreements with the experimental results

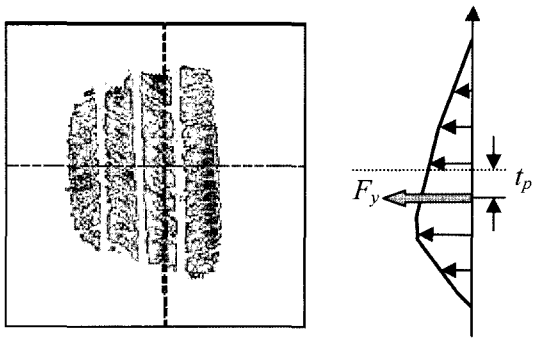

Figure 9. Generation mechanism of lateral force and aligning moment.

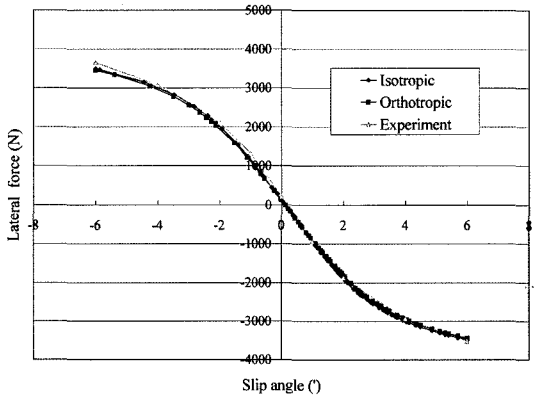

(a) Lateral force vs. slip angle

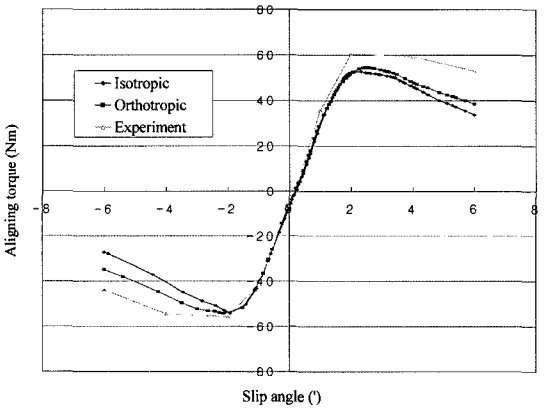

(b) Aligning torque vs. slip angle

Figure 10. Lateral forces and aligning torques according to tread material model.

than those by the isotropic one. However, there exist some differences between calculated aligning torques and experimental ones where the slip angles are larger than 3 degrees. The differences may attribute to the loss of contact patch on a cornering status and the deficiency of torsional stiffness in composite layers. In addition, a

Table 3. The effect of tread material model on force and moment characteristics.

Results	Isotropic tread	Orthotropic tread	Experiment
CC(1°)	0.259	0.250	0.282
CC(4°)	0.746	0.734	0.748
ATC(1°)	8.738	8.830	9.585
ATC(4°)	10.749	11.704	14.164
PRAT[Nm]	−3.325	−2.357	−0.690

direct modeling of tread pattern may be needed to obtain more exact simulation results than those by tread orthotropic model.

Angle effects of tread pattern have been conveniently studied by changing the orientation angle of tread orthotropic moduli. The groove angle is measured as an angle of a lateral groove with respect to the tire axial direction as shown in Figure 3. The angle of the lateral groove is changed by ±15° on each center and shoulder region of tread. The simulation results about the effect of lateral groove angle on force and moment characteristics are summarized in Table 4. It is shown that the groove angle in the tread shoulder region has a more effect on force and moment than that in the tread center region.

7. FRICTIONAL ENERGY SIMULATION

Tire wear originates from frictional energy density distributions on tread surface. The frictional energy density (W) is calculated by multiplying frictional stress (F) by slip (S) at each location on the tread surface in contact with the road surface as follows (Pottinger *et al.*, 1999);

$$W_{ij} = \sum_{k=1}^{n} \{(Fx_{ij}^{k} \cdot Sx_{ij}^{k}) + (Fy_{ij}^{k} \cdot Sy_{ij}^{k})\} \quad (6)$$

Frictional energy densities are simulated using orthotropic tread model. The circumferentially grooved tires with 4 and 5 ribs are respectively modeled for frictional energy simulation. If there exist three circumferential main grooves in tread, the tread is said to have 4 ribs. Frictional energy densities are measured using the Flat Bed test machine developed by Kumho Tire Co. The simulated frictional energy densities are expressed in the unit of lbf/in while the experimental ones are expressed in the unit of volts. Both the simulated and the experimental frictional energy densities are normalized through dividing each value by the average value.

The comparisons of normalized frictional energy densities are plotted in Figure 11 for the tires with 4 ribs and 5 ribs. The frictional energy densities by simulation

Table 4. The effect of lateral groove angle on force and moment characteristics.

(a) The effect of center groove angle change

Model	Reference	CT-15°	CT+15°
Center angle	45.13°	30.13°	60.13°
Shoulder angle	23.48°	23.48°	23.48°
CC(1°)	0.250	0.250	0.249
CC(4°)	0.734	0.736	0.732
ATC(1°)	8.830	8.790	8.820
ATC(4°)	11.704	11.631	11.777
PRAT[Nm]	−2.357	−2.333	−2.436

(b) The effect of shoulder groove angle change

Model	Reference	SH-15°	SH+15°
Center angle	45.13°	45.13°	45.13°
Shoulder angle	23.48°	8.48°	38.48°
CC(1°)	0.250	0.250	0.249
CC(4°)	0.734	0.734	0.733
ATC(1°)	8.830	8.869	8.773
ATC(4°)	11.704	11.769	11.583
PRAT[Nm]	−2.357	-2.975	−2.031

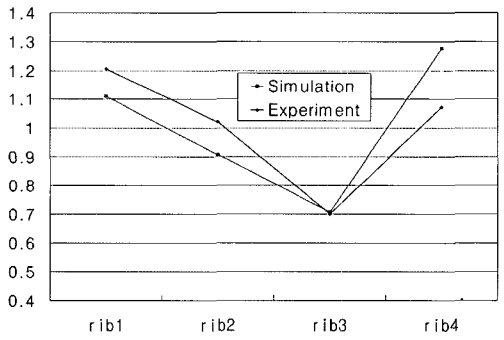

(a) Friction energy densities of tire with 4 ribs

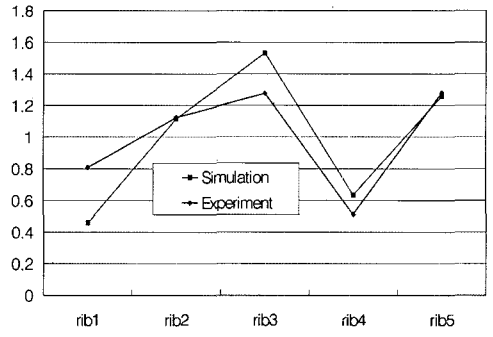

(b) Frictional energy densities of tire with 5 ribs

Figure 11. Comparisons of frictional energy densities by simulation and experiment.

Table 5. Verification of simulation results of frictional energy densities.

(a) 185/70R14 smooth tire with 4 ribs

	Simulation	Experiment
Rib 1	59.46 (1.11)	3.00 (1.21)
Rib 2	48.63 (0.91)	2.54 (1.02)
Rib 3	37.88 (0.71)	1.74 (0.70)
Rib 4	68.41 (1.28)	2.66 (1.07)

(b) 185/70R14 smooth tire with 5 ribs

	Simulation	Experiment
Rib 1	20.58 (0.46)	1.62 (0.81)
Rib 2	50.00 (1.12)	2.26 (1.12)
Rib 3	68.66 (1.53)	2.56 (1.28)
Rib 4	28.50 (0.64)	1.03 (0.51)
Rib 5	56.38 (1.26)	2.57 (1.28)

Note : units are lbf/in in calculation and volts in experiment, and values in parenthesis mean the normalized ones to the average value.

and experiment for each tire are summarized in the Table 5. It is shown that the simulation results of frictional energy densities have very similar tendency with the experimental results. However, there exist some differences between calculated frictional energy densities and experimental ones. Therefore a direct modeling of tread pattern may be needed to obtain more exact simulation results.

8. CONCLUSION

Finite element analysis of a steady-state rolling tire taking the effect of tread pattern into account has been described using a steady-state transport method with ABAQUS. Tread meshes can not fully consider a tread pattern because local detailed tread meshes in the contact region are not allowed in the steady-state transport method. Therefore, the tread elements are modeled to have orthotropic property instead of isotropic property.

The force and moment simulations have been carried out for the cases of both isotropic and orthotropic properties of tread elements. It is shown that the orthotropic case is in a better agreement with the experimental result than the isotropic case. Angle effects of a tread pattern have been studied by changing the orientation angle of orthotropic property of tread. It is shown that the groove angle in the tread shoulder region has a more effect on force and moment than that in the tread center region.

The transient dynamic analysis is now becoming practical with advances in a tread meshing technique of a tire and a computation technology of hardware. Therefore, a direct modeling of tread pattern may be studied to obtain more exact simulation results than those by tread orthotropic model.

REFERENCES

ABAQUS Analysis User's Manual, Version 6.4 (2003). ABAQUS, Inc., Providence, Rhode Island, USA.

Chang, Y. P. and El-Gindy, M. (2005). Virtual prediction of a radial-ply tire's in-plane free vibration modes transmissibility. *Int. J. Automotive Technology* **6**, **2**, 149–159.

Clark, S. K. (1982). *Mechanics of Pneumatic Tires*. U.S. Government Printing Office. Washington, DC. USA.

Danielson, K. T., Noor, A. K. and Green, J. S. (1996). Computational strategies for tire modeling and analysis. *Computers & Structures* **61**, **4**, 673–693.

Faria, L. O., Oden, J. T., Yavari, B., Tworzydlo, W. W., Bass, J. M., and Becker, E. B. (1992). Tire modeling by finite elements. *Tire Science and Technology, TSTCA* **20**, **1**, 33–56.

I-DEAS User's Manual, Version 10.1 (2003). Electronic Data Systems Co., Plano, Texas, USA.

Kim, K. W., Jeong, H. S. and Beom, H. G. (2003). Transient dynamic analysis of a patterned tire rolling over a cleat with an explicit finite element program. *Trans. Korean Society Automotive Engineers* **11**, **6**, 164–177.

Kaliske, M., Zheng, D. and Andre, M. (2002). Formulation of inelastic effects in steady-state rolling tire simulation. *5th World Congress on Computational Mechanics*, Vienna, Austria, 1–10.

Pottinger, M. G. and McIntyre, J. E. (1999). Effect of suspension alignment and modest cornering on the footprint behavior of performance tires and heavy duty radial tires. *Tire Science and Technology, TSTCA*, **27**, **3**, 128–160.